Modelling of a 7-elements GOX/GCH4 Combustion Chamber Using RANS with Coupled Wall Function

By Silong Zhang, Jianfei Wei, Mai Ye AND Oskar J. Haidn

Institute of Advanced Power, Harbin Institute of Technology, No.92 West Da-Zhi Street, 150001, Harbin, China

The report has summarized the preliminary computational work conducted by the the group from Harbin Institute of Technology and the chair of rocket propulsion at TUM. A 7-element rocket combustion chamber using GOX/GCH4 as propellant has been modelled and simulated to get a more comprehensive knowledge of the combustion and heat transfer process. The adequate understanding and accurate prediction of turbulent combustion, heat transfer characteristics are considered key features for the development of reliable oxygen/methane engines. Within the frame of SFB TRR40 program, an experimental test campaign was performed at the chair of rocket propulsion at TUM on a gaseous oxygen (GOX)/gaseous methane (GCH4) combustion chamber with 7-element shear coaxial injectors, and wall heat transfer characteristics were measured. This research aims to build an appropriate CFD model of the 7-Injectors GOX-GCH4 combustion chamber according to the test case provided by the chair of rocket propulsion at TUM to help understand the knowledge and details of the combustion process and heat transfer characteristics inside the chamber. We found that our prediction of pressure distribution along the flow direction agreed with the experiment data well. However, the wall heat flux we got is not so satisfactory, there was about a 30% over prediction than the experiment data. These facts indicate that we have correctly modeled the main chemistry process in the main flow region, but in the near wall region which has great impacts on the heat transfer process, the current model has some defects. After analyzed the results in depth, we incorporated the coupled wall function in our RANS simulations, and the results show that the coupled wall function can improve the prediction of the wall heat load significantly.

1. Introduction

With the rising of commercial aerospace activities, the demanding issues in terms of high operational and handling costs of cryogenic and storable propellants increased the attention for methane/oxygen in the development of future launch vehicles. Methane as a fuel can provide a higher specific impulse, together with better cooling abilities and less soot deposition than kerosene, therefore, methane/oxygen is the most promising propellant combination for the reusable rocket engine [1–3]. Differently than oxygen/hydrogen propellant combination, oxygen/methane can be considered as "space storable" and is favored by higher density, [4] although it gives lower specific impulse. The adequate understanding and accurate prediction of turbulent combustion, heat transfer charac-

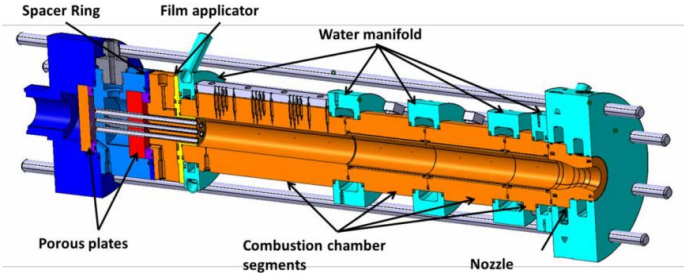

FIGURE 1. Sketch of the experiment configuration [10].

teristics are considered key features for the development of reliable oxygen/methane engines [5].

Within the frame of SFB TRR40 program, an experimental test campaign was performed at the chair of rocket propulsion at TUM on a gaseous oxygen (GOX)/gaseous methane (GCH4) combustion chamber with 7-element shear coaxial injectors. A lot of work has been done to give the prediction of this turbulent combustion process, [6–8] especially about the characteristics of the wall heat load, since the wall heat load is the key parameter which determine the design of the cooling system as well as the duration of the engine directly. Our group also participated in the program, and our numerical results show a reasonable prediction of the reactive process in the chamber [9]. However, the wall heat flux was over predicted about 30% than the experiment data.

In this work, we try to find out the reason for the overestimation of the wall heat flux, and propose a new wall function to correct our previous numerical model. The new wall function shows a good performance for the reactive flow simulation, and the mechanism of the performance is also revealed in this study.

2. Numerical Setups

This section will introduce the reference experiment configuration simulated in this investigation as well as the whole numerical frame adapted in the simulation.

2.1. *Physical model and mesh generation*

The numerical investigation of this paper is based on the standard experiment conducted by Simona et.al at Technical University of Munich [10]. Figure 1 shows the experiment configuration which is a scaled rocket combustion chamber with 7 shear coaxial injectors, the length of the chamber is 341 mm and the inner diameter of the chamber is 30 mm. The chamber is divided into four segments in order to measure the total wall heat flux through the calorimetry method, more detailed information of the configuration can be found in [10].

For simplicity, only the flow domain of the configuration is discretized into computation domain which include injectors, the combustion chamber and the nozzle. In order to improve the computational efficiency, the computational domain is reduced further to 1/6 of its original size. Figure 2 illustrates the computational domain and the cross intersection grids in the chamber part and the nozzle part respectively.

2.2. *Numerical model and boundary conditions*

There are many researches devote to assessing the capability of the RANS method for CFD modeling of turbulent combustion phenomena in a rocket chamber, [11,12] indicat-

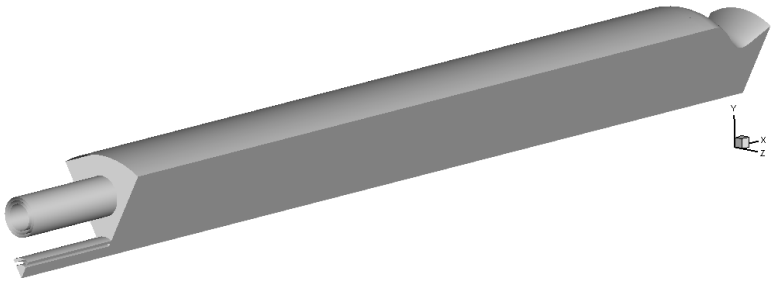

(a) The computational domain.

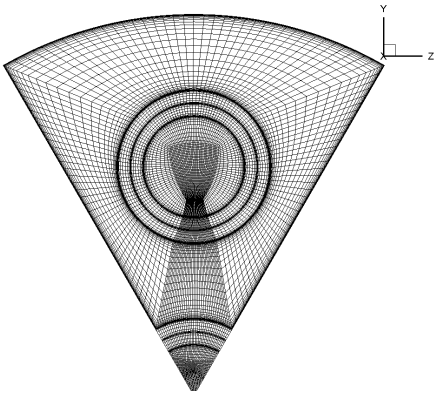

(b) Grids for the chamber part.

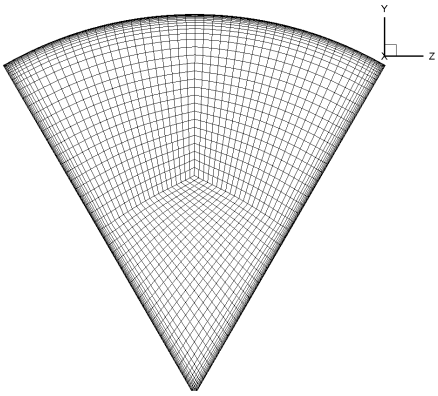

(c) Grids for the nozzle part.

FIGURE 2. Sketch of computational domain.

ing that the simulation based on the RANS framework could get acceptable results with certain accuracy at cost of least time consuming. The whole oxidization rate of methane is much smaller than that of hydrogen due to more complicate reaction routine, and the low temperature near the wall region results from the cooling effect depress the high activation energy chain branching reaction, then further slow down the whole reaction rate. Therefore it is reasonable to consider the GOX/GCH4 combustion phenomena under investigation as a finite-rate reactive flow which can be characterized well by EDC combustion model. The Eddy-Dissipation-Concept (EDC) model developed by Magnusson is an extension of the previous Eddy-Dissipation model to incorporate the detailed chemistry mechanism. The essence of the EDC model is the estimation of the mean reaction rate through phenomenological theory [13] then, the source terms for each species transport equation are determined, and all of the control equations are closed.

The boundary conditions are summarized in Table 1, most of these conditions are specified by the experiment condition, except the nozzle wall and the two symmetric planes. The chamber wall temperature is given by a fitting curve of the discretized experimental data, as shown in Fig.3. The nozzle wall temperature is set to 412 K, since the lack of experimental data and our concerns are the flow and heat transfer process in the chamber part. For simplicity, it is reasonable to set a constant temperature for the nozzle wall, and from the point of continuity, we set the constant to 412 K.

Boundary	Type	Specific	Temperature
Injector GOX	Mass flow	0.211 kg/s	259.4 K
Injector GCH4	Mass flow	0.080 kg/s	237.6 K
Outlet	Pressure outlet	1 bar	-
Injector wall and faceplate	Non slip wall	-	Adiabatic
Combustor chamber wall	Non slip wall	-	Polynomial fitting
Nozzle wall	Non slip wall	-	412 K
Symmetric plane	Symmetry	-	-

TABLE 1. Summary of the boundary conditions.

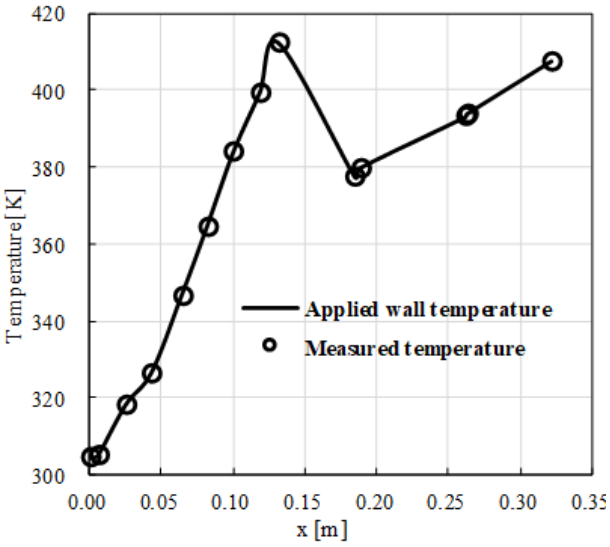

FIGURE 3. The applied wall temperature profile [14].

3. Theoretical Basis for Wall Function

This section will discuss the principles of the wall function, include the origin and implementation of wall function. Then we analysis the special term appears in the wall function when chemistry is taken into account.

3.1. *The origin of general wall function*

Over the past half century, the two equation turbulence models based on Boussinesq hypothesis have been widely used, but most of these models are applicable for high Reynolds number flow, such as the $k-\varepsilon$ model family. In order to handle the low Reynolds number viscous layer appears in the near wall region where high Reynolds turbulence model fails, scholars use the wall function to link the wall flux to the first off-wall grid point parameters directly. The combination of wall functions and the high Reynolds number turbulence model avoids the solution for the viscous layer where very fine gird would be needed when use low Reynolds number turbulence model, result in much less computational cost as well as improvement in computational stability [15].

We go deep into the origin of wall functions from the mathematical perspective. Start-

ing from the general flow process, one seeks for the momentum and energy conservation equations, which are Eq. 3.1 and Eq. 3.2.

$$\frac{\partial \rho \boldsymbol{V}}{\partial t} + \nabla \cdot (\rho \boldsymbol{V}\boldsymbol{V}) = -\nabla P + \nabla \cdot \widetilde{\tau} \tag{3.1}$$

$$\frac{\partial \rho H}{\partial t} + \nabla \cdot (\rho \boldsymbol{V} H) = -\nabla \cdot \boldsymbol{q} + \frac{\mathrm{d}\, P}{\mathrm{d}\, t} + (\widetilde{\tau} : \nabla \boldsymbol{V}) \tag{3.2}$$

The terms in the divergent operator are called flux terms, which contain the convection flux and the diffusion flux, and in the wall adjacent region, the diffusion flux in the direction perpendicular to the wall is much higher than the other two directions which are parallel to the wall, because the diffusion flux vector is generally proportional to the gradient vector. Therefore, we only retain the partial derivative of y which is the coordinate perpendicular to the wall. After the statistical procedure has been applied such as Reynolds time average, the diffusion flux of Eq. 3.1 and Eq. 3.2 are simplified to Eq. 3.3 and Eq. 3.4:

$$\frac{\partial \tau_w}{\partial y} = F \tag{3.3}$$

$$\frac{\partial q_w}{\partial y} = G \tag{3.4}$$

In general, τ_w and q_w depend on the wall quantities as well as outer flow conditions. If F and G are known functions of the distance y, then the Eq. 3.3 and Eq. 3.4 can be integrated over space to generate a formula for momentum flux τ_w and heat flux q_w respectively, these formulas are called law of the wall [16]. The mathematical start point of the wall function is to specify the wall flux through the law of the wall formula directly, and avoid an assumption of quantity profile to discrete the face gradient operator.

More clearly, we start from the general transport equation (Eq. 3.5) for quantity ϕ .

$$\frac{\partial \rho \phi}{\partial t} + \nabla \cdot (\rho \boldsymbol{V} \phi) = \nabla \cdot (k \nabla \phi) + S \tag{3.5}$$

For simplicity, we assume the flow is under steady state condition, and integrate Eq. 3.5 over volume for the two dimensional element P as shown in Fig. 4(a). We first get the semi-discretized equation (Eq. 3.6).

$$\sum_f (\rho \boldsymbol{V} \phi)_f \cdot \boldsymbol{S}_f = \sum_f (k \nabla \phi)_f \cdot \boldsymbol{S}_f + S_V \tag{3.6}$$

Where the subscript f means face quantity, and the summation sign means sum over all the four faces. To complete the discretization, we must assume the quantity distribution profile between two elements to estimate the quantity value and gradient in the face center (ie. the n, w, s, e nodes), because the variables are stored in cell centers (ie. the N, W, S, E nodes).

The simplest way is to assume a linear distribution between two elements. Without losing generality, we focus on the south face. The convection term on the LHS of Eq. 3.6 is discretized to Eq. 3.7.

$$\dot{m}_s \phi_s = \dot{m}_s \frac{\phi_P + \phi_S}{2} \tag{3.7}$$

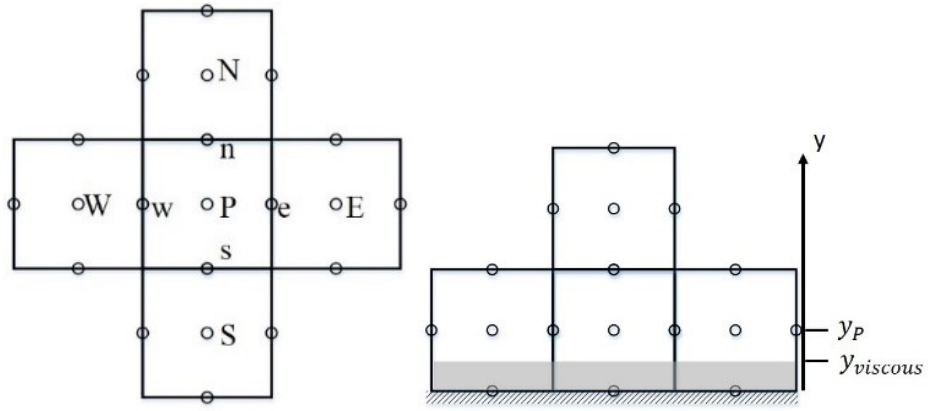

(a) The inner element. (b) The wall adjacent element.

FIGURE 4. Sketch of the space discretization

Also, the diffusion term on the RHS of Eq. 3.6 can be discretized to Eq. 3.8

$$k\nabla\phi_s \cdot S_s = k\frac{(\phi_P - \phi_S)}{\triangle y}\triangle x \tag{3.8}$$

Do the similar discretization process for the other three faces, and combine the coefficient for each cell center quantity, we finally get the algebra equation, as Eq. 3.9

$$a_P\phi_P + \sum_F a_F\phi_F = S_V \tag{3.9}$$

The above process is valid for every inner element which is surrounded by other elements. However, when the element is closed to the wall which is shown in Fig. 4(b), the linear distribution assumption is no longer valid, since the widely known log-law distribution which is highly non-linear caused by the viscous boundary layer, as shown in Fig. 5. That is to say, we can not find a similar way to express the term $k\nabla\phi_s \cdot \boldsymbol{S}_s$ like the Eq. 3.8. The desire to put the first off-wall cell center in the full turbulence region which is the requirement of high Reynolds number turbulence model and the defects of difference scheme to estimate the wall gradient constitute the mathematical start point of wall functions.

To overcome this conflict, one should estimate the term $k\nabla\phi_s \cdot \boldsymbol{S}_s$ from the other way, and clearly, the term has the physical meaning of the quantity diffusion flux that cross the wall. That is to say, the term $k\nabla\phi_s \cdot \boldsymbol{S}_s$ can be estimated directly as the wall stress $\tau_w \cdot \triangle x$ and wall heat flux $-q_w \cdot \triangle x$ for momentum and energy transport equation respectively. Remembering the Eq. 3.3 and Eq. 3.4, if we know the law of the wall, then both the shear stress and the wall heat flux are determined, and the final algebra equation for the wall adjacent element is Eq. 3.10

$$a_P^{'}\phi_P + \sum_F a_F^{'}\phi_F = S_V - (\tau_w\Delta x \ or \ q_w\Delta x) \tag{3.10}$$

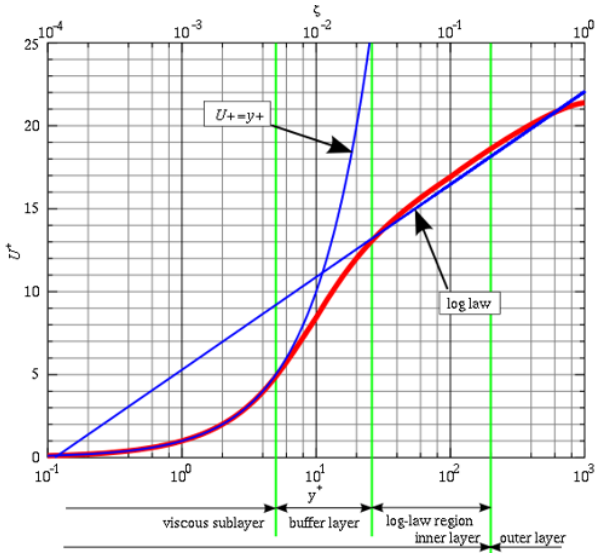

FIGURE 5. The log-law of the wall [17]

3.2. *The origin of coupled wall function*

Coupled wall function is proposed and modeled by Cabrit.O and Nicoud.F through their DNS results for multicomponent reacting turbulent flows. Our work in this investigation is to incorporate the coupled wall function into the commercial CFD software ANSYS FLUENT, then, analysis and access the coupled wall function in the GCH4/GOX turbulence combustion case.

When it comes to the reactive flow circumstance, the momentum and energy equations are the same as Eq. 3.1 and Eq. 3.2 respectively, provided that the chemical enthalpy and the species diffusion velocity are taken into account. We can neglect the transient pressure term and energy dissipation rate term in the Eq. 3.2 due to the low Mach number flow condition in our investigation, and get the Eq. 3.11

$$\rho \frac{\mathrm{d}\, H}{\mathrm{d}\, t} = -\nabla \cdot q \tag{3.11}$$

where $H = \sum_{k=1}^{N} Y_k(h_{f,k}^0 + h_k^s) = H^s + H_f^0$,and $q = -\lambda \nabla T + \rho \sum_{k=1}^{N} Y_k V_{k,D} h_k$.
Expanding the Eq. 3.11to the sense enthalpy form:

$$\rho \frac{\mathrm{d}\, H^s}{\mathrm{d}\, t} = -\nabla \cdot (-\lambda \nabla T + \rho \sum_k Y_k \boldsymbol{V}_{k,D} h_k^s) - [\rho \frac{\mathrm{d}\, H_f^0}{\mathrm{d}\, t} + \nabla \cdot (\rho \sum_k Y_k \boldsymbol{V}_{k,D} h_{f,k}^0)] \tag{3.12}$$

Combined with the species transport equation (Eq. 3.13), the term in the square bracket of Eq. 3.12 can be simplified to Eq. 3.14.

$$\frac{\partial \rho Y_k}{\partial t} + \nabla \cdot (\rho \boldsymbol{V} Y_k) + \nabla \cdot (\rho Y_k \boldsymbol{V}_{k,d}) = \dot{\omega}_k \tag{3.13}$$

$$\rho \frac{\mathrm{d}\, H_f^0}{\mathrm{d}\, t} + \nabla \cdot (\rho \sum_k Y_k \boldsymbol{V}_{k,D} h_{f,k}^0) = \sum_k h_{f,k}^0 \dot{\omega}_k \tag{3.14}$$

Clearly, the term in the square bracket has the physical meaning of the conversion rate of the chemical energy to heat, or simply, the heat release rate. Then, similar to the Eq. 3.4, the heat flux in the divergence operator is only retained the derivation of y direction, the following equation is obtained:

$$\frac{\partial q_w}{\partial y} = \sum_k h^0_{f,k}\dot{\omega}_k \tag{3.15}$$

Unlike the classic wall functions where G is zero which is deduced with no chemistry assumption, and it is easy to see that, if the species production rate $\dot{\omega}_k$ in Eq. 3.15 are all zeros, Eq. 3.15 degenerates to Eq. 3.4. Although Eq. 3.15 has a compact form, the heat release term is still an unknown function of y, we can not obtain an explicit formula to determine the wall heat flux. Now we go back to Eq. 3.11 which is the conservation of mixture specific enthalpy, after the time averaging procedure, one end up with a more convenient expression:

$$\frac{\partial \overline{q_w}}{\partial y} = \frac{\partial}{\partial y}(\overline{\rho}\widetilde{\nu''h''_s} + \overline{\rho}\sum_k \widetilde{\nu''Y''_k}h^0_{f,k} - \overline{\lambda\frac{\mathrm{d}\,T}{\mathrm{d}\,y}} + \overline{\rho}\sum_k\{h_kY_kV_{k,y}\}) \tag{3.16}$$

Because the mixture specific enthalpy include the chemical formation enthalpy, thus the heat release rate term does not appear explicitly as a source term in the RHS of Eq. 3.11.

Thanks to the DNS results given in the Ref. [16], the last two terms in the brackets of Eq. 3.16 can be neglected compared to the first two terms, then the remaining two second order moment terms can be modeled based on the Boussinesq hypothesis. For the turbulent flux of sensible enthalpy $\overline{\rho}\widetilde{\nu''h''_s}$.

$$\overline{\rho}\widetilde{\nu''h''_s} \approx -\lambda_t\frac{\mathrm{d}\,\overline{T}}{\mathrm{d}\,y} = -\frac{\mu_t C_P}{Pr_t}\frac{\mathrm{d}\,\overline{T}}{\mathrm{d}\,y} \tag{3.17}$$

And for the turbulent flux of chemical enthalpy $\overline{\rho}\widetilde{\nu''Y''_k}\triangle h^0_{f,k}$:

$$\overline{\rho}\sum_k \widetilde{\nu''Y''_k}h^0_{f,k} \approx \sum_k -\frac{\mu_t}{Sc_t}\frac{\mathrm{d}\,\overline{Y}_k}{\mathrm{d}\,y}h^0_{f,k} \tag{3.18}$$

Bring the Eq. 3.17 and Eq. 3.18 back to the Eq. 3.16, we obtain the following model for the wall heat flux:

$$\overline{q_w} = -\frac{\mu_t C_P}{Pr_t}\frac{\mathrm{d}\,\overline{T}}{\mathrm{d}\,y} + \sum_k -\frac{\mu_t}{Sc_t}\frac{\mathrm{d}\,\overline{Y}_k}{\mathrm{d}\,y}h^0_{f,k} \tag{3.19}$$

The chemical enthalpy term in the Eq. 3.19 will be further discussed in the next section, and the mechanism of this coupled wall function is explained. Cabrit and Nicoud gave the final coupled wall function in the form of wall units, thus T^+, and test the efficiency of the new wall function in their priori DNS/LES tests:

$$T^+ = K(Pr) + \frac{a}{B_q}u^+ \tag{3.20}$$

Where $K(Pr)$ is a quite complicated function of Prandtl number and determined by least square method, and the coefficient before u^+ is :

$$\frac{\alpha}{B_q} = \frac{C_p}{\frac{C_p}{Pr_t} + \frac{1}{Sc_t}\sum_k \frac{\mathrm{d}\,\overline{Y_k}}{\mathrm{d}\,\overline{T}} h^0_{f,k}} \tag{3.21}$$

Reference [16] is recommended for more information. To calculate the wall heat flux from the wall function, we can invert the Eq. 3.20 according to the definition of T^+:

$$q_w = \frac{-\rho C_p u^*}{T^+}(T_c - T_w) \tag{3.22}$$

3.3. *The implementation of coupled wall functions*

The implementation of the coupled wall function to the ANSYS FLUENT is conducted by user defined function (UDF) way, and mainly divided to three sequential parts. The first part is using $DEFINE\_ADJUST$ macro to calculate all the coefficients that will be accessed in the following macros, the second part is using $DEFINE\_HEAT\_FLUX$ macro to determine the wall heat flux and return the value to the slover, the last part is using $DEFINE\_EXECUTE\_AT\_END$ to monitor the key values in the calculation for debugging. Data is stored in user defined memory (UDM) and accessed by C_UDMI macro.

Special treatment is needed when calculate the derivative term in Eq. 3.21, since this term represents the change rate of species mass fraction with the temperature when the mixture is at chemical equilibrium condition. Importing the data of that thermodynamic properties into the UDF is quiet cumbersome and restricts by the resolution required. Instead, we assume that the products of GOX/GCH4 are near the chemical equilibrium condition, thus, the derivative can be approximated as follows:

$$\frac{d\overline{Y_k}}{d\overline{T}} = \frac{\nabla\overline{Y_k}\cdot\boldsymbol{n}}{\nabla\overline{T}\cdot\boldsymbol{n}} \tag{3.23}$$

Where n is the unit vector perpendicular to the wall surface. Besides, we adapted the Eq. 3.24 to calculate u^* rather than its definition to improve the stability of simulation process.

$$u^* = \frac{u_P u_k}{u_\tau^2} \tag{3.24}$$

4. Results and Discussion

4.1. *Validation of the coupled wall functions*

From the previous analysis, we recognize that, if chemical reactions do not occur in the flow process, the coupled wall function should degenerate to the standard wall function. That is to say, the standard wall function and the new coupled wall function should give the same results for the pure flow and heat transfer process. Based on this fact, we set the validation cases as a two dimensional pure mixing process of GOX and GCH4. The computational domain is shown in Fig.6, which is similar to the combustion chamber simulated in this investigation, except the inclined chamber wall. The first off-wall gird is adjusted to ensure $y^+ \approx 30$, since the coupled wall function is modeled in the full turbulent region, and the total length of the domain is 80 mm. The two comparative cases both adapt the standard $k-\varepsilon$ model to close the second order moment in turbulence,

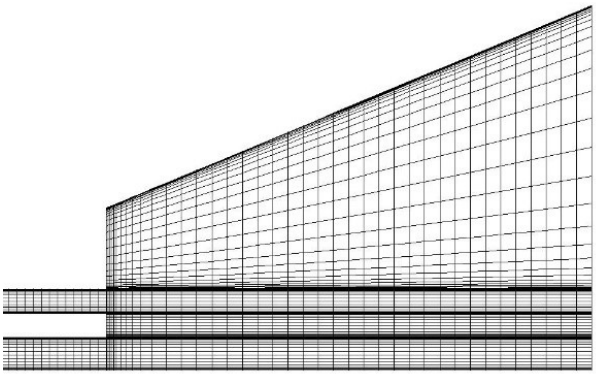

FIGURE 6. Grids for the validation case

Boundary	Type	Specific	Temperature
GOX inlet	Velocity inlet	2 m/s	300 K
GCH4 inlet	Velocity inlet	2 kg/s	300 K
Outlet	Pressure outlet	1 bar	-
Injector wall and faceplate	Non slip wall	-	Adiabatic
inclined wall	Non slip wall	-	800K
Symmetric line	Symmetry	-	-

TABLE 2. boundary conditions for validation case

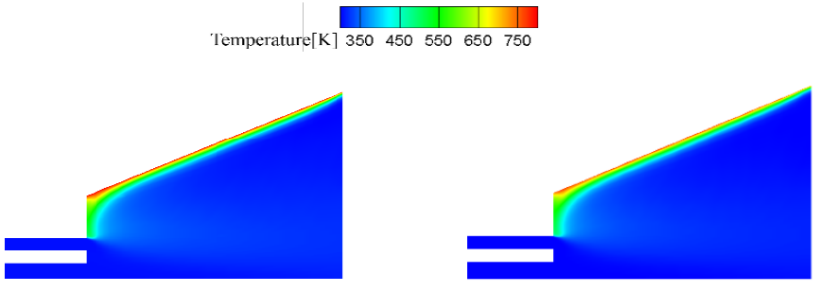

FIGURE 7. Temperature contours for the validation cases

with the one combined with the standard wall function, and the other combined with the coupled wall function.

The boundary conditions are summarized in Table 2. In a word, the validation cases are pure mixing and heat transfer process, the temperature contours of the two cases are shown in Fig. 7, and the wall heat flux profile is illustrated in Fig. 8.

4.2. *The results of the combustion chamber using the coupled wall functions.*

Three cases for comparison are set according to Table 3. All the cases use the standard $k-\varepsilon$ model combined with the EDC combustion model and the chemical mechanism

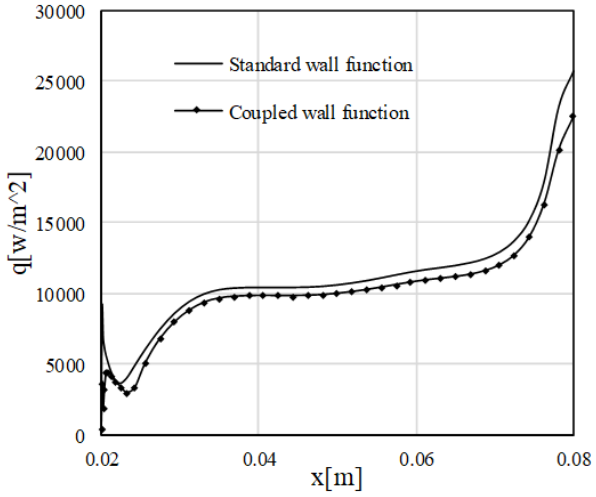

FIGURE 8. wall heat flux for the validation case

Case	Wall treatment	Mesh y^+
1	Enhanced wall treatment	1
2	Coupled wall function	30
3	Enhanced wall treatment	30

TABLE 3. The cases setup for the investigation.

from Dong Gang, the Prandtl number is set to 0.85 and the Schmidt number is set to 0.7.

The average heat flux profiles of the chamber wall for the three cases are shown in Fig. 9. The results are impressive, the prediction of the wall heat flux is improved remarkably compared to that of the case 1, which is investigated thoroughly in our previous work.

However, the heat flux for the front part of the chamber wall ($x < 145mm$) and the nozzle part are still not so satisfactory. The unchanged prediction for the nozzle part is the result of not enabling the new coupled wall function in that section, since what we are interested in is the chamber wall heat load. The puzzling thing is a little higher prediction of the heat flux in the front part compared to the case 1, although the deviation is small. Unlike the rest part ($x > 145mm$), the heat flux of the front part is quiet insensitive to the first off-wall grid distance as well as the wall functions adapted. Since the law of the wall for the velocity of the coupled wall functions is the same as that of the enhanced wall treatment, we suppose that, the overestimation of the heat flux in the front part for the three cases is caused by the defects in the velocity wall function, because, there exist a recirculation zone near the wall in the front part, and therefore, the adverse pressure gradient may needs to be considered. There still needs further investigation to reveal the mechanism for the overestimation of the heat flux in the front part of the chamber wall.

We confirm that, the impacts of the coupled wall function are restricted in the near wall

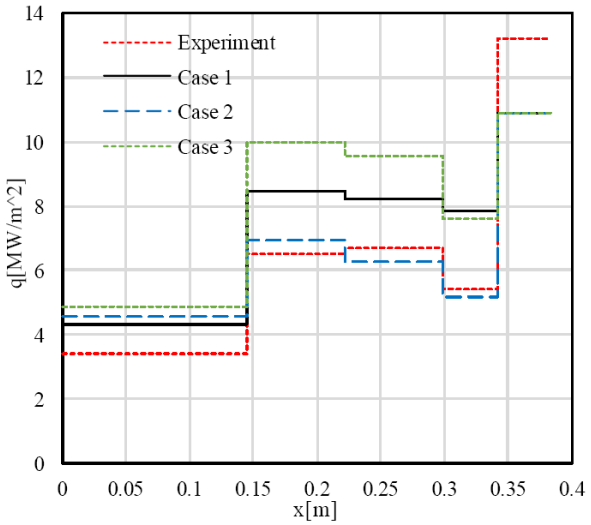

FIGURE 9. The average wall heat flux for the three numerical cases.

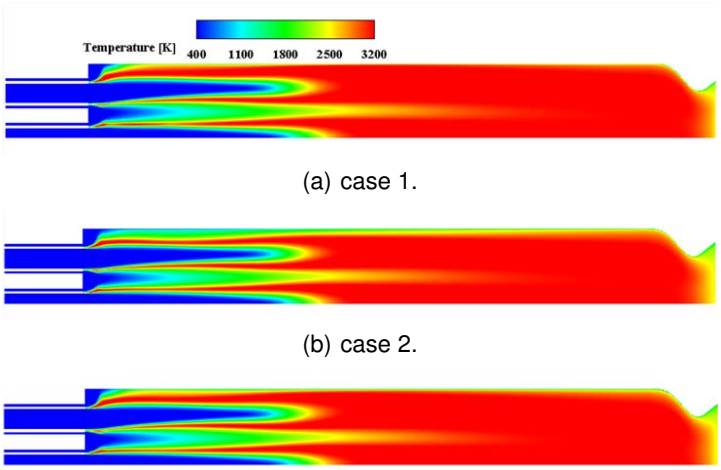

(a) case 1.

(b) case 2.

(c) case 3.

FIGURE 10. temperature contours for the three cases

region, the properties of the main flow is unchanged as shown in the following figures. From Fig. 10, which is the temperature contours in the middle slice of the three cases, we can clearly see that the temperature field is unchanged for the main flow. For the case 2, the boundary layer of the temperature is slightly extended, so the temperature gradient near the wall is smooth than that of case 1 and case 3, therefore, the heat flux prediction of case 2 is decreasing. Besides, the near wall flame in the front part of the case 2 is thinner than the other cases, but the heat flux of that part is overestimated, this puzzling facts may be caused by the three dimensional effects, and as stated earlier, the near wall flow and heat transfer process in the front part need further investigation.

Figure 11 shows the pressure profiles of the three cases, the profiles show a good

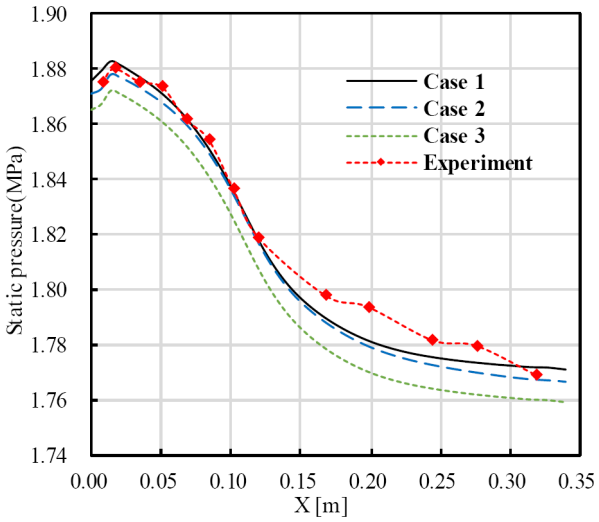

FIGURE 11. pressure profiles for the three cases

agreement with the experimental data, which is another evidence to prove the capacity of our numerical frame to capture the overall characteristics of the turbulent combustion phenomena. Figure 12 shows the heat release rate of the chemistry which is represented by the RHS of Eq. 3.15, the heat release rate of the three cases are almost the same with each other. The heat release rate reaches a peak value about $7\,GW/m^3$ and then hold for a distance about 30 mm. In this region, the flame is ignited by the flame stable zone after the injector post, but restricted by the finite mixing layer developed by the shear flow of the coaxial injectors, thus the amount of reactants well mixed to combustion is maintained to a low level. After a certain distance about 50 mm, the mixing layer is quickly expanded in the combustion chamber, and the amount of reactants well mixed to combustion is also increasing, thus, the heat release reaches to a second peak value about $16\,GW/m^3$, this point, where the combustion is the most violent, is also the inflexion point of the pressure distribution, means the mixing region expands to the maximum, and the combustion is almost complete after this point.

4.3. *The mechanism of the coupled wall function.*

In the previous section, we show the results of using the coupled wall function, and confirm that the coupled wall function can improve the prediction of the wall heat flux considerably, now we try to explain the mechanism of the coupled wall function behind its function.

We come back to the Eq. 3.19, the additional second term in the brackets of the Eq. 3.19 takes the chemistry effects into account, and it is the core of the coupled wall function. The physical meaning of the term is clear, it is a directional derivative in the y direction for the chemical enthalpy of the mixture. From the Le Chatelier principle, we conclude that when the mixture approach the low temperature wall, the chemical equilibrium point will shift to the low chemical enthalpy direction, and the mixture will release heat due to the equilibrium shifting effects. That means the second term in the Eq. 3.19 is negative, the same as the first term, this case will result in a larger value of the heat flux which is contrary to the predicted results.

The reason for this paradox is ignoring the three dimensional effects in our simulation.

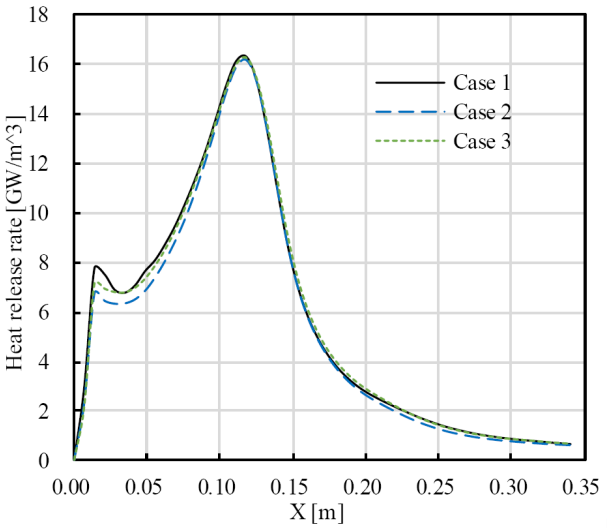

FIGURE 12. volume heat release rate profiles for the three cases

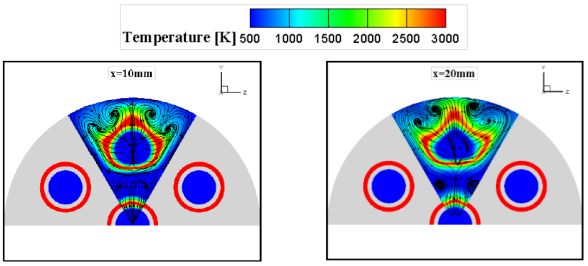

FIGURE 13. stream trace for the two cross slices

For more clearly, we rewrite the second term in the Eq. 3.19 in the cylindrical coordinate system:

$$\sum_k \frac{dY_{\overline{k}}}{dy} h^0_{f,k} = \sum_k \frac{d\overline{Y_k}}{dr} h^0_{f,k} = \sum_k \frac{d\overline{Y_k}}{dt} \frac{\mathrm{d}\, t}{\mathrm{d}\, r} h^0_{f,k} = \frac{\sum_k h^0_{f,k} \dot{\omega_k}}{V_r} = \frac{Q_c}{V_r} \tag{4.1}$$

The stream trace of the cross slices in the chamber is illustrated in the Fig. 13, we can clearly see that the radical velocity is rather complicate due to the three dimensional effects and the interaction of the injectors. The radical velocity can be positive or negative which will directly change the sign of the Eq. 4.1. Therefore it is important to assess the net contribution to the wall heat flux of the Eq. 4.1.

We calculate the gradients of the species mass fraction for the main species, and show the y-components of the gradients in the Fig. 14, we clearly see that, the y-components of species mass fraction gradients are rather non-uniform in the circumferential direction, the three dimensional effects are profound.

To assess the net contribution of the Eq. 4.1 on the wall heat flux, we should evaluate the order of magnitude for the Eq. 4.1. The area average of the gradients is collected in Table 4.

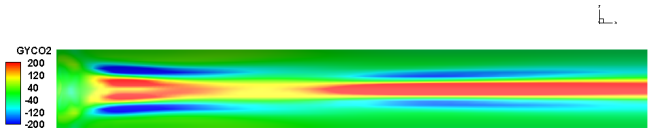

(a) y-component of mass fraction gradient for CO_2

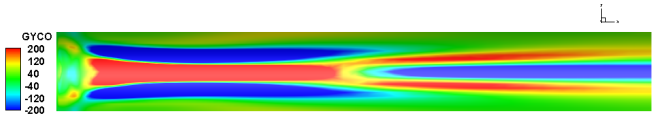

(b) y-component of mass fraction gradient for CO

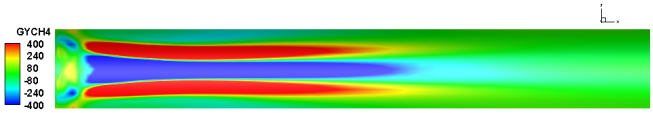

(c) y-component of mass fraction gradient for CH_4

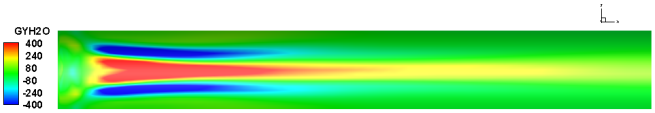

(d) y-component of mass fraction gradient for H_2O

FIGURE 14. gradient contours for the main species

Species	Area average of gradients	Chemical enthalpy $h^0_{f,k}[MJ/kg]$
CO_2	-1.18	-8.94
CO	-4.43	-13.4
CH_4	9.68	-4.65
H_2O	-3.81	-3.95

TABLE 4. Data for the main species

The inner product of the column 2 and the column 3 of Table 4 is about $4 \times 10^7 J/kg$, the value is positive, so the net contribution of the second term in the Eq. 4.1 is to lower the prediction of the wall heat flux. Further more, the order of the magnitude of the μ_t near the wall region is about 10^{-2}, therefore, the total effect of the chemistry on the wall heat flux is about $4 \times 10^5 W$, which is comparable to the initial prediction of $10^6 W$. That means the chemical effects on the wall heat flux in the GOX/GCH4 turbulent combustion case can not be neglected and that is the main reason for the 30% overestimation of wall heat flux in the previous investigation.

5. Conclusions

A 7-element rocket combustion chamber using GOX/GCH4 as propellant has been modeled and simulated. The initial numerical frame using enhanced wall treatment can capture the main characteristics of the combustion process in the chamber, while the

prediction of the wall heat flux is overestimate by 30% compared to the experimental data. To remedy and explain this defect of our numerical frame, we introduce the coupled wall function by simplifying the Navier-Stokes equations and replacing the turbulent term by their model counterpart. The new coupled wall function can take the chemistry effects into account, and degrades to the classical formulation when the flow is a pure mixing process without chemical reaction.

It is practical to implement the coupled wall function using UDFs based on the FLUENT platform, and the calculation gives reasonable results compared to the experimental data, the more accurate prediction of the wall heat flux is the most obvious, and the prediction of the pressure distribution is also improved a little. However, the wall heat flux in the front part of the chamber wall has little profit from the coupled wall function, and even a little worse. The mechanism behind this puzzle may hide in the flow condition of the recirculation zone, and still needs further investigation. We also confirm that the impacts of the coupled wall function on the main flow properties are negligible, the pressure and the total volume heat release rate distribution of the main flow are almost the same for both the enhanced wall treatment and the coupled wall function.

Finally, we explain the mechanism of the coupled wall function to include the chemistry effects. The impacts of the chemistry on the wall heat flux are the coupling effects of two physical phenomenon, one is the heat release rate caused by the chemical reaction, or more precisely, the chemical equilibrium shifting by the large temperature gradient. And the other is the radical velocity, which represents the powerful vortex system caused by the interaction between the jets and the wall in the combustion chamber. We also estimate the magnitude of the chemical effects on the wall heat flux, and confirm that the turbulent flux of the chemical enthalpy is comparable to the turbulent flux of the sensible enthalpy in the GOX/GCH4 combustion circumstance, ignoring the chemical effects will result in an overestimation of the wall heat flux just as the previous unsatisfactory results.

Acknowledgments

Financial support has been provided by the German Research Foundation (Deutsche Forschungsgemeinschaft – DFG) in the framework of the Sonderforschungsbereich Transregio 40.

References

[1] PRECLIK, D., HAGEMANN, G., KNAB, O., MADING, C., HAESELER, D., HAIDN, O., WOSCHNAK, A. AND DEROSA, M. (2005). LOX-hydrocarbon preparatory thrust chamber technology activities in germany. In: *41st AIAA/ASME/SAE/ASEE Joint Propulsion Conference & Exhibit*. 4555.

[2] BUCCHI, A., BRUNO, C. AND CONGIUNTI, A. (2005). Transpiration cooling performance in LOX/methane liquid-fuel rocket engines. *Journal of Spacecraft and Rockets*, **42**(3), 476–486.

[3] LUX, J. AND HAIDN, O. (2009). Flame stabilization in high-pressure liquid oxygen/methane rocket engine combustion. *Journal of Propulsion and Power*, **25**(1), 15–23.

[4] PREUSS, A., PRECLIK, D., MADING, C., GORGEN, J., SOLLER, S., HAIDN, O., OSCHWALD, M., CLAUSS, W., ARNOLD, R. AND SENDER, J. (2008). LOx/Methane technology efforts for future liquid rocket engines. In: *Space Propulsion Conference*.

[5] NEILL, T., JUDD, D., VEITH, E. AND ROUSAR, D. (2009). Practical uses of liquid methane in rocket engine applications. *Acta Astronautica*, **65**(5-6), 696–705.

[6] PERAKIS, N., RAHN, D., EIRINGHAUS, D. AND HAIDN, O.J. (2018). Heat transfer and combustion simulation of a 7-element gox/gch4 rocket combustor. In: *2018 Joint Propulsion Conference*. 4554.

[7] ZIPS, J., TRAXINGER, C., BREDA, P. AND PFITZNER, M. (2019). Assessment of presumed/transported probability density function methods for rocket combustion simulations. *Journal of Propulsion and Power*, **35**(4), 747–764.

[8] RAHN, D., RIEDMANN, H., BEHR, R. AND HAIDN, O.J. (2018). Non-adiabatic flamelet modeling for the numerical simulation of methane combustion in rocket thrust chambers. In: *2018 Joint Propulsion Conference*. 4869.

[9] PERAKIS, N., HAIDN, O.J., EIRINGHAUS, D., RAHN, D., ZHANG, S., DAIMON, Y., KARL, S. AND HORCHLER, T. (2018). Qualitative and quantitative comparison of rans simulation results for a 7-element GOX/GCH4 rocket combustor. In: *2018 Joint Propulsion Conference*. 4556.

[10] SILVESTRI, S., KIRCHBERGER, C., SCHLIEBEN, G., CELANO, M.P. AND HAIDN, O. (2018). Experimental and numerical investigation of a multi-injector gox-gch4 combustion chamber. *Transactions of the Japan Society for Aeronautical and Space Sciences, Aerospace Technology Japan*, **16**(5), 374–381.

[11] ZHUKOV, V.P. (2015). Computational fluid dynamics simulations of a GO2/GH2 single element combustor. *Journal of Propulsion and Power*, **31**(6), 1707–1714.

[12] CHEMNITZ, A., SATTELMAYER, T., ROTH, C., HAIDN, O., DAIMON, Y., KELLER, R., GERLINGER, P., ZIPS, J. AND PFITZNER, M. (2016). Numerical investigation of flow and combustion in a single-element gch4/gox rocket combustor: Aspects of turbulence modeling. In: *52nd AIAA/SAE/ASEE Joint Propulsion Conference*.

[13] MAGNUSSEN, B. (1981). On the structure of turbulence and a generalized eddy dissipation concept for chemical reaction in turbulent flow. In: *19th Aerospace Sciences Meeting*. 42.

[14] SILVESTRI, S., LUNGU, P., KIRCHBERGER, C.U. AND HAIDN, O.J. (2018). Axial and azimuthal heat load distribution in 7-injector gox/gch4 combustion chamber. In: *2018 Joint Propulsion Conference*. 4552.

[15] JAEGLE, F., CABRIT, O., MENDEZ, S. AND POINSOT, T. (2010). Implementation methods of wall functions in cell-vertex numerical solvers. *Flow, turbulence and combustion*, **85**(2), 245–272.

[16] CABRIT, O. AND NICOUD, F. (2009). Direct simulations for wall modeling of multicomponent reacting compressible turbulent flows. *Physics of Fluids*, **21**(5).

[17] BARANYI, P. https://en.wikipedia.org/wiki/Law_of_the_wall. Accessed April 4, 2019.